Precise measurement of the $e^+e^- \to \pi^+\pi^-(\gamma)$ cross section with the initial state radiation method at BABAR

WANG Wen-Feng(王文峰)[1]) (for the BABAR collaboration)

University of Notre Dame; SLAC, 2575 Sand Hill Road, Menlo Park, CA 94025, USA

Abstract We present a precise BABAR measurement on the cross section of the process $e^+e^- \to \pi^+\pi^-(\gamma)$ from threshold to an energy of 3 GeV with the initial state radiation (ISR) technique, using 232 fb^{-1} of data collected with the BABAR detector at e^+e^- center-of-mass energies near 10.58 GeV. The ISR luminosity is determined from a study of the leptonic process $e^+e^- \to \mu^+\mu^-\gamma(\gamma)$. The leading-order hadronic contribution to the muon magnetic anomaly calculated using the $\pi\pi$ cross section measured from threshold to 1.8 GeV is $(514.1 \pm 2.2(\text{stat}) \pm 3.1(\text{syst})) \times 10^{-10}$.

Key words pion form factor, ISR, g-2, BABAR

PACS 13.40Em, 13.60.Hb, 13.66.Bc

1 Introduction

Precise measurements of the $e^+e^- \to$ hadrons cross section are necessary to evaluate dispersion integrals for calculations of hadronic vacuum polarization (VP). Of particular interest is the contribution a_μ^{had} to the muon magnetic moment anomaly a_μ, which requires data in a region dominated by the process $e^+e^- \to \pi^+\pi^-(\gamma)$. Approximately 73% contribution arises from this process alone which is the leading contributor to the uncertainty of the theoretical prediction for a_μ. Comparison of the theoretical and measured [1] values of a_μ shows a discrepancy of about 3σ when current e^+e^- data [2–4] are used, possibly hinting at new physics. An approach using τ decay data corrected for isospin-breaking, leads to a smaller difference [5].

This analysis is base on 232 fb^{-1} of data recorded with the BABAR detector [6] at the PEP-II asymmetric-energy e^+e^- storage rings. Charged-particle tracks are measured with a five-layer double-sided silicon vertex tracker (SVT) together with a 40-layer drift chamber (DCH) inside a 1.5 T superconducting solenoid magnet. The energy and direction of photons are measured in the CsI(Tl) electromagnetic calorimeter (EMC). Charged-particle iden-

tification (PID) uses ionization loss dE/dx in the SVT and DCH, the Cherenkov radiation detected in a ring-imaging device (DIRC), and the shower deposit in the EMC (E_{cal}) and in the instrumented flux return (IFR) of the magnet.

Signal and background ISR processes are simulated with Monte Carlo (MC) event generators based on Ref. [7]. Additional ISR photons are generated with the structure function method [8], and additional FSR photons with PHOTOS [9]. Background events from $e^+e^- \to q\bar{q}$ (q=u,d,s,c) are generated with JETSET [10]. The response of the BABAR detector is simulated with GEANT4 [11].

2 Analysis

2.1 Method overview

The results on $\pi\pi$ production [12] presented here are obtained with the Initial State radiation (ISR) method [13] using e^+e^- annihilation events collected at a center-of-mass (CM) energy $\sqrt{s}$ near 10.58 GeV. The cross section for $e^+e^- \to X$ at the reduced energy $\sqrt{s'} = m_X$, where X can be any final state, is deduced from a measurement of the radiative process $e^+e^- \to X\gamma$ where the photon is emitted by the e^+ or

e⁻; $s' = s(1 - 2E_\gamma^*/\sqrt{s})$, where E_γ^* is the CM energy of the ISR photon. In this analysis, $\sqrt{s'}$ ranges from threshold to 3 GeV. Two-body ISR processes with $X = \pi^+\pi^-(\gamma)$ and $X = \mu^+\mu^-(\gamma)$ are measured, where the ISR photon is detected at large angle and the charged particle pair can be accompanied by a final state radiation (FSR) photon. The $\pi\pi$ cross section are obtained from the ratio of pion to muon yield. In this way several common factors cancel (e⁺e⁻ integrated luminosity (L_{ee}), additional ISR, vacuum polarization and ISR photon efficiency), and significantly reducing the systematic uncertainty. In addition the measured muon cross section is compared to the QED prediction, termed the QED test, providing an important cross check of this analysis.

The $\sqrt{s'}$ spectrum of e⁺e⁻ → Xγ events is related to the cross section for the process e⁺e⁻ → X through

$$\frac{dN_{X\gamma}}{d\sqrt{s'}} = \frac{dL_{ISR}^{eff}}{d\sqrt{s'}} \varepsilon_{X\gamma}(\sqrt{s'}) \sigma_X^0(\sqrt{s'}) , \qquad (1)$$

where $\varepsilon_{X\gamma}$ is the detection efficiency (acceptance) determined by simulation with corrections obtained from data, and σ_X^0 is the bare cross section (excluding VP). The measurement of $\sigma_{\pi\pi(\gamma)}^0$ uses the effective ISR luminosity $dL_{ISR}^{eff}/d\sqrt{s'}$ provided by the measured mass spectrum of $\mu\mu\gamma(\gamma)$ events following Eq. (1) in which $\sigma_X^0(\sqrt{s'})$ is the $\mu\mu(\gamma)$ bare cross section computed with QED [14]. The relevant Feynman diagrams are given in Fig. 1.
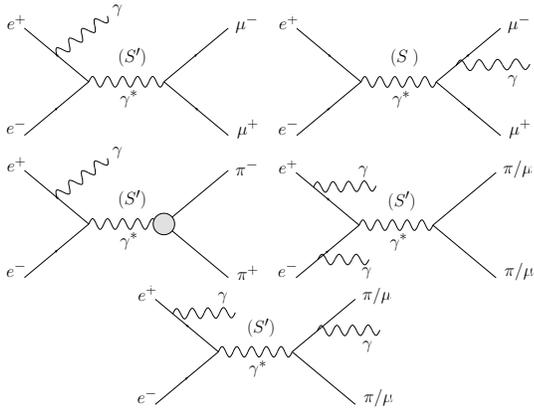

Fig. 1. The Feynman diagrams for the processes relevant to this study: lowest-order (LO) ISR μμ (top left), LO FSR μμ (top right), LO ISR ππ (middle left), next-to-leading order (NLO) ISR with additional ISR (middle right), NLO with additional FSR (bottom). The process LO FSR ππ is not shown here as it is strongly suppressed at 10.58 GeV.

For the QED test, the measurement of $\sigma_{\mu\mu(\gamma)}^0$ uses the effective ISR luminosity definition as a product of the e⁺e⁻ integrated luminosity (L_{ee}), the radiator function [13], the ratio of detection efficiencies for the ISR photon in data and simulation (not included in $\varepsilon_{X\gamma}$), and the VP correction $(\alpha(s')/\alpha(0))^2$. The radiator function, determined by the simulation, is the probability to radiate one or several ISR photons so that the produced final state X (excluding ISR photons) has mass $\sqrt{s'}$.

2.2 Event selection and particle related corrections

Two-body ISR events are selected by requiring a photon with $E_\gamma^* > 3$ GeV and laboratory polar angle in the range 0.35–2.40 rad, and exactly two tracks of opposite charge, each with momentum $p > 1$ GeV/c and within the angular range 0.40–2.45 rad. If several photons are detected, the ISR photon is chosen to be that with the highest E_γ^*. The charged-particle tracks, required to have at least 15 hits in the DCH, must originate within 5 mm of the collision axis and extrapolate to DIRC and IFR active areas which exclude low-efficiency regions. An additional criterion based on a combination of E_{cal} and dE/dx reduces electron contamination.

Acceptance and mass-dependent efficiencies for trigger, reconstruction, PID, and event selection are computed using the simulation. The ratios of data and MC efficiencies have been determined from specific studies, as described below, and are applied as mass-dependent corrections to the MC efficiency. They amount to at most a few percent and are known to a few permil level or better.

Tracking and PID efficiencies are determined taking advantage of pair production. For tracking studies, two-prong ISR candidates are selected on the basis of the ISR photon and one track. A kinematic fit yields the expected parameters of the second track. The unbiased sample of candidate second tracks is used to measure track reconstruction efficiency. The maximum correlated two-track loss induced by track overlap in the DCH is 0.6% for pions and 0.3% for muons.

Tracks are assigned uniquely to a complete set of PID classes using a combination of cut-based and likelihood selectors. The 'μ' class is addressed first by making use of track IFR penetration and hit spread distribution, and of the E_{cal} value. Tracks failing the 'μ' identification are labeled as 'e' if they satisfy $E_{cal}/p > 0.8$. The 'K' class is determined using DIRC information and dE/dx. Remaining tracks are labeled as 'π'. A tighter selection called 'π_h' is ap-

plied in mass regions where background dominates or to create a pure pion test sample.

Efficiencies for PID are measured from pure samples of muon, pion, and kaon pairs obtained from $x\overline{x}\gamma$ events where one track is selected as 'μ', 'π_h', or 'K' and the other is used to probe the PID algorithm. The efficiencies are stored, according to momentum and position in the IFR or the DIRC. Typical efficiency for 'μ' is 90%, with 10% mis-ID as 'π'. The 'π' efficiency is strongly momentum-dependent because of mis-ID as 'K' (1% at 1 GeV/c, reaching 20% at 6 GeV/c), as 'μ' (5%–6%), or as 'e' (2%). Correlations between the PID efficiencies, due to track overlap, have been observed and parametrized. They are largest for muons where the correlated PID loss reaches 1.3% of the events below 1 GeV/c^2. It is important to control this effect, since it affects the $\pi\pi$ and $\mu\mu$ samples in an anti-correlated way.

To obtain the spectra N_{jj} of produced particle pairs of true type j, a set of three linear relations must be solved. They involve the N_{jj}, the measured mass distributions for each 'ii'-identified final state, and the probabilities ε_{ii}^{ij}, (i, j = μ, π or K) which represent the product of the measured efficiencies for each track of true type j to be identified as 'i', corrected by correlation factors.
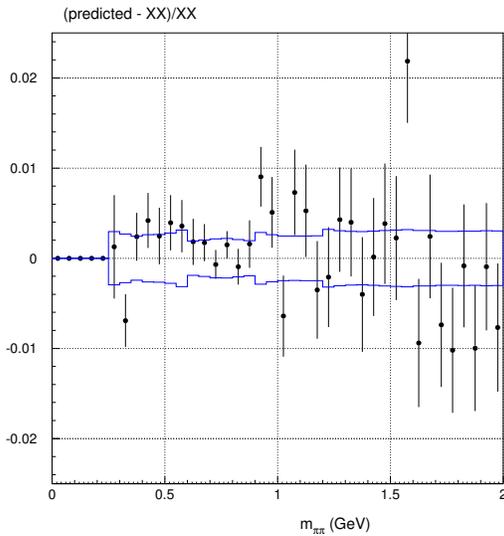

Fig. 2. The global PID test on data: relative difference between the PID-predicted total spectrum, ($N_{\mu\mu} + N_{\pi\pi} + N_{KK} + N_{ee}$ background), and the measured one without PID applied. The estimated systematic uncertainties are shown by the blue band.

A global consistency check of the PID corrections is done by comparing the sum of the N_{ii} spectra to the measured mass spectrum before PID. Fig. 2 shows the relative difference between the measured spectrum without PID and the predicted one from the 'diagonal' 'ii' spectra and the measured corrections. Agreement is observed, with deviations statistically compatible with the estimated systematics from all the PID efficiency determinations, typically 3×10^{-3}.

2.3 Kinematic fit and background subtraction

A contribution ($< 10^{-3}$) to $N_{\pi\pi}$ from $p\bar{p}\gamma$ is estimated from MC and subtracted after reweighting the rate to agree with the BABAR measurement [15]. Multi-hadronic background from $e^+e^- \rightarrow q\bar{q}$ comes from low-multiplicity events in which an energetic γ originating from a π^0 is mistaken as the ISR photon candidate. To normalize this rate from JETSET, the π^0 yield obtained by pairing the ISR photon with other photons in the event is compared in data and MC; JETSET overestimates this background by a factor 1.3. Multi-hadronic ISR backgrounds are dominated by $e^+e^- \rightarrow \pi^+\pi^-\pi^0\gamma$ and $e^+e^- \rightarrow \pi^+\pi^-2\pi^0\gamma$ contributions. An approach similar to that for $q\bar{q}$ is followed to calibrate the background level from the 3π ISR process, using ω and ϕ signals. The ratio of data to MC yield is found to be 0.99 ± 0.04. The MC estimate for the $2\pi2\pi^0\gamma$ process is used and assigned a 10% systematic uncertainty. A residual radiative Bhabha background is identifiable only near threshold and at large mass, where the pion signal vanishes. Its magnitude is estimated from the helicity angle distribution in the $\pi\pi$ CM frame at low energy and its energy dependence obtained from a control sample of radiative Bhabha events. It is assigned a 100% systematic uncertainty. To suppress the contribution from the $e^+e^- \rightarrow \gamma\gamma$ process with a photon conversion, which affects the spectrum at threshold, the vertex of the two tracks is required to be closer than 5 mm to the collision axis in the transverse plane. This criterion is applied only to events in the ρ tails, defined to lie outside the central region $0.5 < m_{\pi\pi} < 1.0$ GeV/c^2. Background contributions to the $N_{\mu\mu}$ spectrum are negligible.

Each event is subjected to two kinematic fits to the $e^+e^- \rightarrow X\gamma$ hypothesis, where X includes one additional photon, detected or not. Both fits use the ISR photon direction and the parameters and covariance matrix of each charged-particle track. The energy of the ISR photon is not used, as it has little impact for the relatively low CM energies involved. The two-constraint (2C) 'ISR' fit allows an undetected photon collinear with the collision axis, while the 3C 'FSR' fit uses any photon with $E_\gamma > 25$ MeV.

When more than one such photon is present, the best 'FSR' fit is retained. An event with no extra photon is characterized only by its χ^2_{ISR} value. Most events have small χ^2 values for both fits; an event with only a small χ^2_{ISR} (χ^2_{FSR}) indicates the presence of additional ISR (FSR) radiation. Events where both fits have large χ^2 values result from track or ISR photon resolution effects, the presence of additional radiated photons, or multi-hadronic background. To accommodate the expected background levels, different criteria in the ($\chi^2_{\text{ISR}}, \chi^2_{\text{FSR}}$) plane are applied depending on the $m_{\pi\pi}$ mass regions. For the central ρ region, a loose 2D contour has been optimized to remove the main background area while maintaining control of the associated systematic uncertainties. The same procedure is used in the $\mu\mu\gamma$ analysis in spite of the very small background. In the ρ tails, a tighter χ^2 selection is imposed to reduce the larger background. Samples of 529320 pion and 445631 muon events are selected in the mass range below 3 GeV/c^2, where the $m_{\pi\pi}$ ($m_{\mu\mu}$) mass is calculated from the best 'ISR' or 'FSR' fit.

The computed acceptance and the χ^2 selection efficiency depend on the description of radiative effects in the generator. The FSR rate is measured from events that satisfy the 'FSR' fit, with an additional photon ($E_\gamma > 0.2$ GeV) within 20° of either track. The excess in data relative to the generator prediction using PHOTOS [9] is $(-4\pm6)\%$ of total FSR for muons, and $(21\pm5)\%$ for pions. This difference results in a $(6\pm2)\times10^{-4}$ correction. More significant differences are found between data and the generator for additional ISR photons, since the latter uses a collinear approximation and an energy cut-off for very hard photons. Induced kinematical effects have been studied using the next-to-leading order (NLO) PHOKHARA generator [17] at four-vector level with fast simulation. Differences in acceptance occur at the few percent level, and these yield corrections to the QED test. In contrast, since radiation from the initial state is common to the pion and muon channels, the $\pi\pi(\gamma)$ cross section, obtained from the $\pi\pi/\mu\mu$ ratio, is affected and corrected only at a few permil level. Additional ISR effects on the χ^2 selection efficiencies factorize in both processes and cancel in the ratio. The χ^2 selection efficiency determined from muon data applies to pions, after correction for the effect of secondary interactions and the π/μ difference for additional FSR. Therefore the measurement of the pion cross section is to a large extent insensitive to the description of NLO effects in the generator.

2.4 Measurement of $\sigma(e^+e^- \to \mu^+\mu^-(\gamma))$ and comparison with QED

The QED test involves two additional factors, both of which cancel in the $\pi\pi/\mu\mu$ ratio: L_{ee} and the ISR photon efficiency, which is measured using a $\mu\mu\gamma$ sample selected only on the basis of the two muon tracks. The QED test is expressed as the ratio of data to the simulated spectrum, after the latter is corrected using data for all known detector and reconstruction differences. The generator is also corrected for its known NLO deficiencies using the comparison to PHOKHARA. The ratio is consistent with unity from threshold to 3 GeV/c^2, (Fig. 3(a)). A fit to a constant value yields ($\chi^2/n_{\text{df}} = 55.4/54$; n_{df}=number of degrees of freedom)

$$\frac{\sigma^{\text{data}}_{\mu\mu\gamma(\gamma)}}{\sigma^{\text{NLO QED}}_{\mu\mu\gamma(\gamma)}} - 1 = (40\pm20\pm55\pm94)\times10^{-4}, \quad (2)$$

where the errors are statistical, systematic from this analysis, and systematic from L_{ee}, respectively. The QED test is thus satisfied within an overall accuracy of 1.1%.

2.5 Unfolding

To correct for resolution and FSR effects, an unfolding of the background-subtracted and efficiency-corrected $m_{\pi\pi}$ distribution is performed. A separate mass-transfer matrix is created using simulation for the ρ central and tail regions; this provides the probability that an event generated in a $\sqrt{s'}$ interval i is reconstructed in a $m_{\pi\pi}$ interval j. The matrix is corrected using data to account for the larger rate of events with poorer mass resolution. Performance and robustness of the unfolding method [18] have been assessed using test models. For the 2-MeV intervals, the significant elements of the resulting covariance matrix lie near the diagonal over a typical range of 6–8 MeV, which corresponds to the energy resolution.

3 Results

The results for the $e^+e^- \to \pi^+\pi^-(\gamma)$ bare cross section [19] including FSR, $\sigma^0_{\pi\pi(\gamma)}(\sqrt{s'})$, are given in Fig. 3(b). Prominent features are the dominant ρ resonance, the abrupt drop at 0.78 GeV due to ρ-ω interference, a clear dip at 1.6 GeV resulting from higher ρ state interference, and additional structure near 2.2 GeV. Systematic uncertainties are estimated from the precision of the data-MC comparisons and from the measurement procedures used for the various efficiencies. They are reported in Table 1 for $0.3 < \sqrt{s'} < 1.2$ GeV. Although larger outside this

range, the systematic uncertainties do not exceed statistical errors over the full spectrum for the chosen energy intervals.
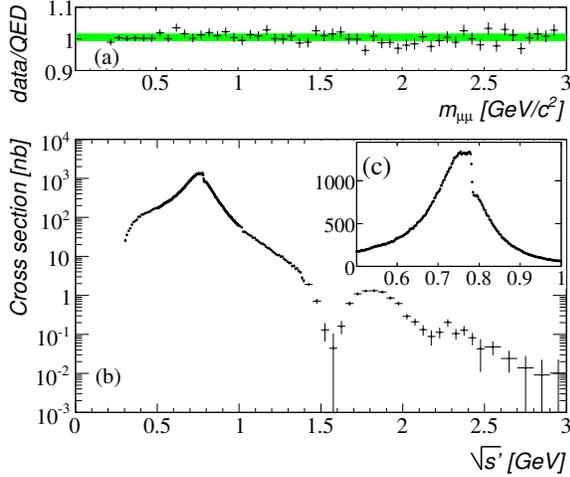

Fig. 3. (a) The ratio of the measured cross section for $e^+e^- \rightarrow \mu^+\mu^-\gamma(\gamma)$ to the NLO QED prediction. The band represents Eq. (2). (b) The measured cross section for $e^+e^- \rightarrow \pi^+\pi^-(\gamma)$ from 0.3 to 3 GeV. (c) Enlarged view of the ρ region in energy intervals of 2 MeV. The errors are from the combined diagonal elements of the statistical and systematic covariance matrices.

The square of the pion form factor is defined as usual by the ratio of the dressed cross section without FSR, divided by the lowest-order cross section for point-like spin 0 charged particles. Thus,

$$|F_\pi|^2(s') = \frac{3s'}{\pi\alpha^2(0)\beta_\pi^3}\,\sigma_{\pi\pi}(s') \qquad (3)$$

with

$$\sigma_{\pi\pi}(s') = \frac{\sigma^0_{\pi\pi(\gamma)}(s')}{1+\dfrac{\alpha(0)}{\pi}\eta(s')}\left(\frac{\alpha(s')}{\alpha(0)}\right)^2. \qquad (4)$$

The FSR correction [21, 22] $\alpha/\pi\,\eta(s')$ is slowly varying with s' and amounts to 8.0×10^{-3} at the ρ mass. A standard vector-dominance model (VDM) is used to fit the the measured form factor, including resonances ($\rho(770)$, ρ', ρ'') and ρ-ω interference, shown at Fig. 5.
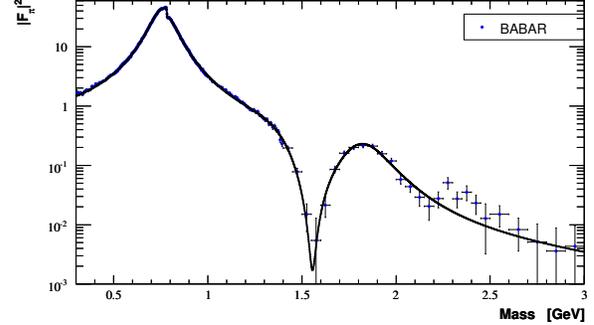

Fig. 4. The pion form factor squared as a function of the $\pi^+\pi^-$ mass from 0.3 to 3 GeV and the VDM fit described in the text.
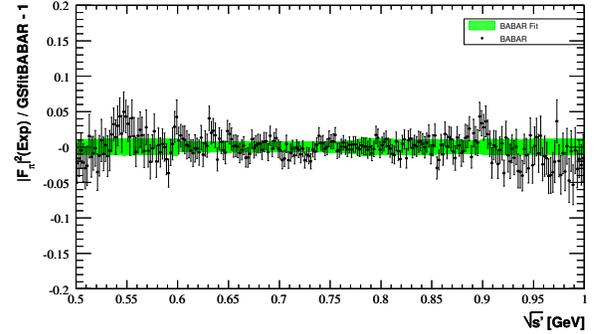

Fig. 5. The relative difference between the measured pion form factor squared and the VDM model fit in the mass range 0.5 to 1 GeV. The width of the band shows the propagation of statistical errors in the fit and quoted systematic uncertainties, quadraticaly.

Table 1. Relative systematic uncertainties (in 10^{-3}) on the $e^+e^- \rightarrow \pi^+\pi^-(\gamma)$ cross section by $\sqrt{s'}$ intervals (in GeV) up to 1.2 GeV. The statistical part of the efficiency uncertainties is included in the total statistical uncertainty in each interval.

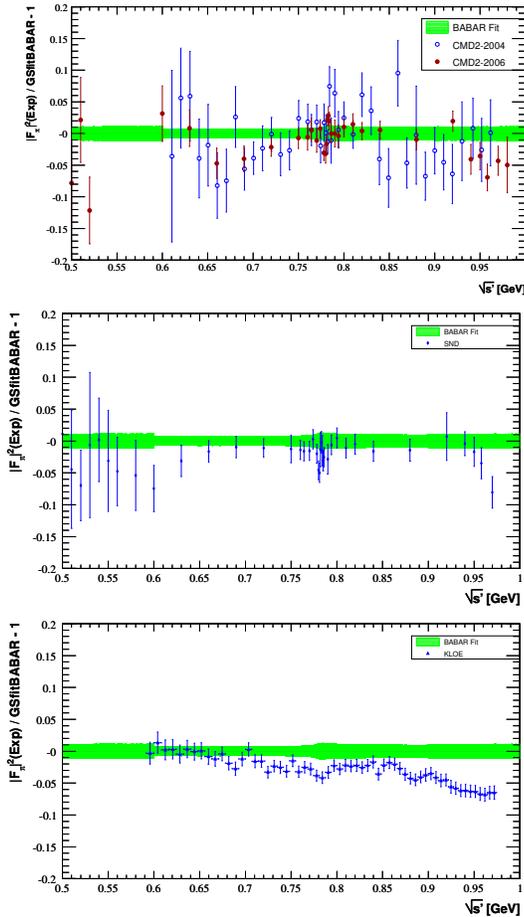| source of uncertainty	CM energy interval/GeV				
	0.3–0.4	0.4–0.5	0.5–0.6	0.6–0.9	0.9–1.2
trigger/ filter	5.3	2.7	1.9	1.0	0.5
tracking	3.8	2.1	2.1	1.1	1.7
π-ID	10.1	2.5	6.2	2.4	4.2
background	3.5	4.3	5.2	1.0	3.0
acceptance	1.6	1.6	1.0	1.0	1.6
kinematic fit (χ^2)	0.9	0.9	0.3	0.3	0.9
correlated $\mu\mu$ ID loss	3.0	2.0	3.0	1.3	2.0
$\pi\pi/\mu\mu$ non-cancel.	2.7	1.4	1.6	1.1	1.3
unfolding	1.0	2.7	2.7	1.0	1.3
ISR luminosity ($\mu\mu$)	3.4	3.4	3.4	3.4	3.4
total uncertainty	13.8	8.1	10.2	5.0	6.5

Fig. 6. The relative difference of form factor squared from the $e^+e^- \to \pi^+\pi^-$ between the BABAR fit and the previous e^+e^- experiments in the 0.5–1 GeV mass region: CMD-2 (top), SND (middle) and KLOE (bottom). Systematic and statistical uncertainties are included for both results, with the diagonal elements of the BABAR covariance matrix. For all results, the diagonal elements of the BABAR covariance matrix reprented by the green band.

The measured form factor can be compared to published data from the CMD-2 and SND experiments in Novosibirsk, KLOE in Frascati, in the mass range between 0.5 and 1 GeV, shown in Fig. 6. The agreement is reasonable with Novosibirsk within systematic errors, while poor with KLOE above the ρ peak.

The lowest-order contribution of the $\pi\pi(\gamma)$ intermediate state to the muon magnetic anomaly is given by

$$a_\mu^{\pi\pi(\gamma),\mathrm{LO}} = \frac{1}{4\pi^3} \int\limits_{4m_\pi^2}^{\infty} \mathrm{d}s'\, K(s')\, \sigma_{\pi\pi(\gamma)}^0(s') \,, \qquad (5)$$

where $K(s')$ is a known kernel [20]. The integration uses the measured cross section and the errors are computed using the full statistical and systematic covariance matrices. The systematic uncertainties for each source are taken to be fully correlated over all mass regions. The integrated result from threshold to 1.8 GeV is

$$a_\mu^{\pi\pi(\gamma),\mathrm{LO}} = (514.1 \pm 2.2 \pm 3.1) \times 10^{-10} \,, \qquad (6)$$

where the errors are statistical and systematic. This value is larger than that from a combination of previous e^+e^- data [5] (503.5 ± 3.5), but is in good agreement with the updated value from τ decay [5] (515.2 ± 3.4).

In summary, the cross section for the process $e^+e^- \to \pi^+\pi^-(\gamma)$ has been measured in the energy range from 0.3 to 3 GeV, using the ISR method. The result for the $\pi\pi$ hadronic contribution to a_μ has a precision comparable to that of the combined value from existing e^+e^- experiments. However, the BABAR central value is larger, which reduces the deviation of the direct a_μ measurement from the Standard Model prediction.

References

1   Bennett G W et al. Phys. Rev. D, 2006, **73**: 072003
2   Aulchenko V M et al. JETP Lett., 2005, **82**: 743; JETP Lett., 2006, **84**: 413; Akhmetshin R R et al. Phys. Lett. B, 2007, **648**: 28
3   Achasov M N et al. JETP, 2006, **103**: 380
4   Ambrosino F et al. Phys. Lett. B, 2009, **670**: 285
5   Davier M et al. arXiv:0906.5443
6   Aubert B et al. Nucl. Instr. Meth. A, 2002, **479**: 1
7   Czyż H, Kühn J H. Eur. Phys. J. C, 2001, **18**: 497
8   Caffo M, Czyż H, Remiddi E. Nuo. Cim. A, 1997, **110**: 515
9   Barberio E, van Eijk B, Was Z. Comput. Phys. Comm., 1991, **66**: 115
10   Sjöstrand T. Comput. Phys. Commun., 1994, **79**: 74
11   Agostinelli S et al. Nucl. Instr. Meth. A, 2003, **506**: 250

12   Aubert B et al. Phys. Rev. Lett., 2009, **103**: 231801
13   Arbuzov A B et al. J. High Energy Phys., 1998, **9812**: 009; Binner S, Kühn J H, Melnikov K. Phys. Lett. B, 1999, **459**: 279
14   Correction for the effect of lowest-order FSR is applied
15   Aubert B et al. Phys. Rev. D, 2006, **73**: 012005
16   Aubert B et al. Phys. Rev. D, **70**: 072004
17   Czyż H et al. Eur. Phys. J. C, 2004, **35**: 527; Eur. Phys. J. C, 2005, **39**: 411
18   Malaescu B. arXiv:0907.3791
19   A file containing the cross section data and their covariance matrices is provided in the EPAPS depository (E-PRLTA0-103-045950)
20   Brodsky S J, de Rafael E. Phys. Rev., 1968, **168**: 1620
21   Bystritskiy Yu M et al. hep-ph/0505236
22   Czyż H et al. Eur. Phys. J. C, 2005, **39**: 411